ACS OMEGA

Article

Cite This: ACS Omega 2019, 4, 5172−5179

http://pubs.acs.org/journal/acsodf

Carrierless Immobilization Route for Highly Robust Metal−Organic Hybrid Enzymes

Andoni Rodriguez-Abetxuko,[†] Maria C. Morant-Miñana,[†,§] Mato Knez,[†,‡] and Ana Beloqui*[,†]

[†]CIC nanoGUNE, Av. Tolosa, 76, E-20018 Donostia/San Sebastian, Spain

[‡]IKERBASQUE, Basque Foundation for Science, Maria Diaz de Haro 3, E-48013 Bilbao, Spain

Supporting Information

ABSTRACT: The absence of a universal enzyme immobilization method that fulfils the needs of each biocatalytic system has boosted the development of new approaches to the fabrication of heterogeneous biocatalysts. Herein, we present a protocol for the synthesis of a novel sort of catalytically responsive hybrid biomaterials, named metal−organic enzyme aggregates (MOEAs). The formation of MOEAs is triggered by the coordination of divalent metal cations to imidazole-decorated enzyme nanogels in a fast and effective assembly mechanism. The size and morphology of MOEAs can be tailored from small individual particles to macroscopic aggregates, which are stable in water and disassemble in the presence of a complexing agent. Finally, the extensive compositional and catalytic characterization of the hybrids showed high transformation rates, significant protein loads, and great thermostability. These features revealed MOEAs as an excellent alternative as carrierless immobilization system.

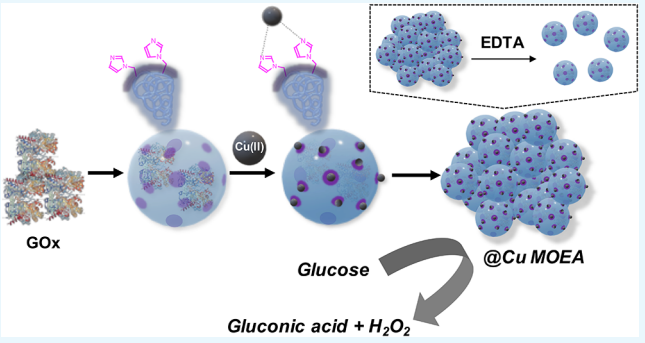

1. INTRODUCTION

The development of new and more efficient tools for the immobilization of enzymes has attracted increasing interest in the last years.[1−3] As compared to solubilized form, confined enzymes usually show improved features such as stability and resistance in harsh operational conditions and ease of reusability.[4−7] Hence, the selection of a robust, stable, and efficient biocatalytic support platform has become a major research avenue. In this regard, solid porous inorganic or organic materials, e.g., ordered mesoporous materials, have been successfully used as high-loading enzyme immobilization solid supports.[8,9] The techniques used for the immobilization of proteins on those materials are based on interfacial physical or chemical bonding to the surface or the formation of cross-linked aggregates inside the pores. However, as pure physical interactions may cause the desorption of enzymes under particular conditions, the covalent approach could damage the protein structure. Inspired by the affinity of distinct residue side chains such as histidines, cysteines, lysines, and asparagines toward metal cations (mainly Ni, Cu, Co, and Zn), the coordination of metal cations to proteins can be used as a reversible and less-harmful cross-linking method for enzyme immobilization.[10−13] As an example, his-tagged recombinant proteins are easily tethered to nitrilotriacetic acid derivatized supports through metal−cation chelation.[14,15] Yet, requirements of computational and molecular biology tools make the production of recombinant proteins a complex and lengthy process, thus alternative approaches for metal-driven protein assembly are needed. Interestingly, the addition of methylimidazole (analogue to side-chain residue of His residues) and metal cations, i.e., Zn(II), to a protein solution leads to the in situ growth of zeolitic-imidazolate (ZIF-8) metal−organic frameworks (MOFs) in which the enzyme remains embedded into a supramolecular structure.[16−18] The MOF−enzyme composites have demonstrated enormous potential in technological and industrial applications.[19] Moreover, as comparable studies have shown, the distribution of enzymes within the ZIF-8 crystal is dependent on the utilized synthetic conditions.[20] Hence, several synthesis approaches have been released in the last years.[21−26] However, there are still some challenges, such as the reduction of incubation time, the increase of protein loadings, and the achievement of high-efficiency approaches, to overcome in this field. Indeed, typical examples of enzyme−MOF composites synthesized in the absence of organic solvents usually lead to the growth of huge amount of noncatalytic support material and low-protein loadings (1−10 wt %), which cause catalytic diffusion issues.[24]

The synthesis of polymer−protein conjugates has become an expanding research field for the development of new methods for enzyme immobilization and stabilization.[27−29] Several approaches, i.e., encapsulation, entrapment, cross-linking, and covalent bonding, are attempted to immobilize enzymes on polymeric supports.[30−32] In this work, we show the utilization of imidazole-bearing enzyme−polymer nanoconjugates for the

Received: December 19, 2018
Accepted: February 26, 2019
Published: March 12, 2019

DOI: 10.1021/acsomega.8b03559
ACS Omega 2019, 4, 5172−5179

Scheme 1. Proposed Experimental Workflow for the Synthesis of MOEAs[a]

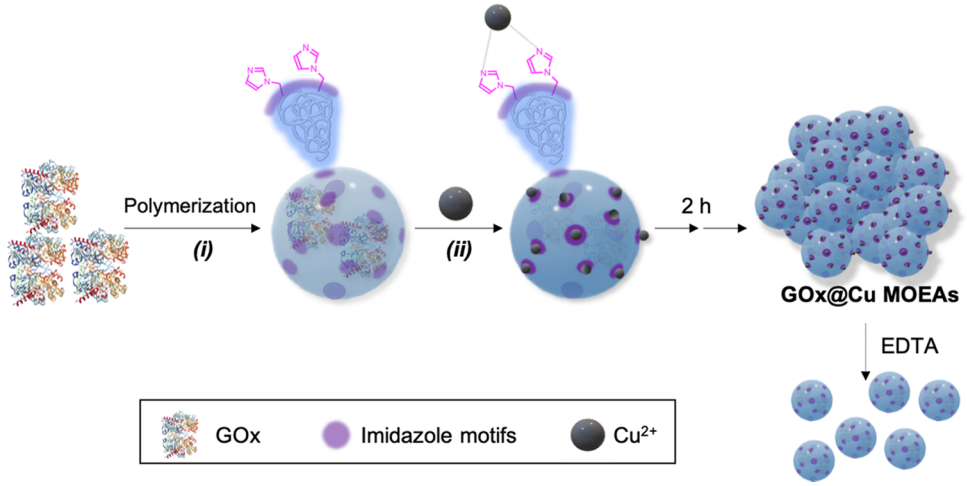

[a]Enzymes are encapsulated into imidazole-modified nanogels (i), which are assembled by coordination to metal ions (ii). MOEA particles are retrieved after 2 h and can be disassembled by the action of strong complexing agents, i.e., ethylenediaminetetraacetic acid (EDTA).

fabrication of carrierless metal−organic catalytic biomaterials in aqueous media. The functional role of polymer in this system is 2-fold: (i) ensuring the confinement of multiple imidazole molecules around the protein and (ii) imparting stability to the enzyme under harsh operational conditions. Hence, the exposure of imidazole molecules linked to the enzyme−polymer nanoconjugates allows the metal-directed assembly of those into hybrid clusters, herein termed metal−organic enzyme aggregates (MOEAs) (Scheme 1). The features and performance of MOEAs are deeply studied and compared to those of ZIF-8−enzyme composites.

2. RESULTS AND DISCUSSION

2.1. Synthesis and Characterization of Imidazole-Decorated Protein−Polymer Nanoconjugates. As mentioned above, our approach seeks to artificially encircle enzymes with multiple imidazole motifs. For this reason, we have developed a one-step straightforward route to synthesize imidazole-bearing enzyme, i.e., glucose oxidase (GOx), nanogels. Native GOx was mixed with acrylamide (AAm), *N*,*N*′-methylenebisacrylamide, and vinyl imidazole (VIm) comonomers in the presence of radical initiators (ammonium persulfate and *N*,*N*,*N*′,*N*′-tetramethylethylenediamine) under diluted conditions (Scheme 1i).[29] The synthesis conditions were optimized to both maximize the presence of imidazole entities and prevent the uncontrolled aggregation and precipitation of the nanogels (see Materials and Methods section for detailed information). Stable GOx nanogels (GOx@imNG) were prepared employing a protein/VIm molar ratio of 1−1000 (Figure S1).

Atomic force microscopy (AFM) of isolated particles (Figure 1A) revealed an oval GOx@imNG and confirmed a hydrodynamic diameter of ∼25 nm as measured by dynamic light scattering (DLS) (Figure S2). Moreover, circular dichroism measurements on GOx@imNG showed that the secondary structure of the protein within the nanogel is retained (Figure S3). The embedment of the protein within the nanogel is also evidenced by attenuated total reflectance Fourier transform infrared (ATR-FTIR) spectroscopy. We detected a broader and more intense amide I infrared band of the GOx@imNG sample, which also shifted from 1632 to 1642

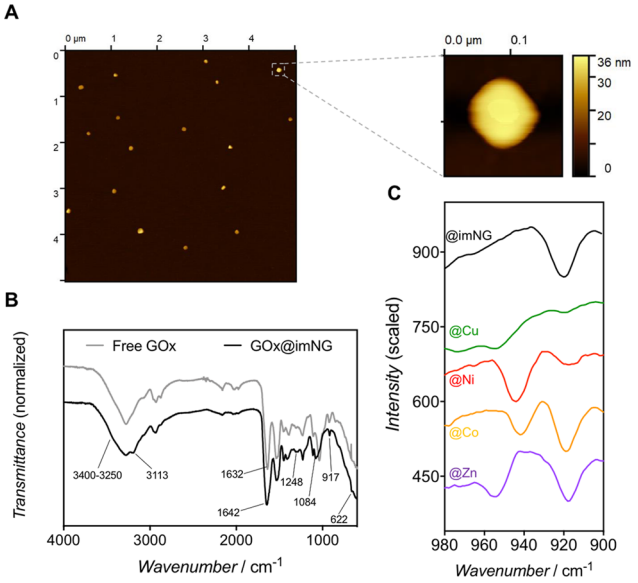

Figure 1. Structural characterization of imidazole nanogels: size and morphology of GOx@imNG sample were revealed by AFM (A). Chemical characterization of free protein, imidazole nanogels, and MOEAs: infrared spectra of GOx@imNG compared to that of free GOx sample (B) and zoomed-in infrared spectra, in the 900−980 cm^{-1} spectral window, of GOx@imNG nanogels and @Cu, @Ni, @Co, and @Zn MOEAs (C). The peaks denoting the presence of the polymer and the embedment of the protein inside the poly(AAm-*co*-VIm) nanogel are highlighted.

cm^{-1} in comparison to free GOx (Figure 1B). This effect can be explained by the overlap of one of the characteristic bands of polyacrylamide polymer, which settles at 1644 cm^{-1}, with the amide I band of the protein.[33] Moreover, slight modifications in the secondary structure of the biomolecule, provoked by the intermolecular interactions between the polymer backbone and the protein, might also contribute to broaden the infrared peak.[34] Furthermore, the formation of a polymeric network is confirmed by the polyacrylamide N−H stretching vibrations in the 3250−4000 cm^{-1} infrared region and a new band at 1084 cm^{-1} attributed to the terminal polyvinyl groups.[35] Besides, the presence of imidazole motifs

DOI: 10.1021/acsomega.8b03559
ACS Omega 2019, 4, 5172−5179

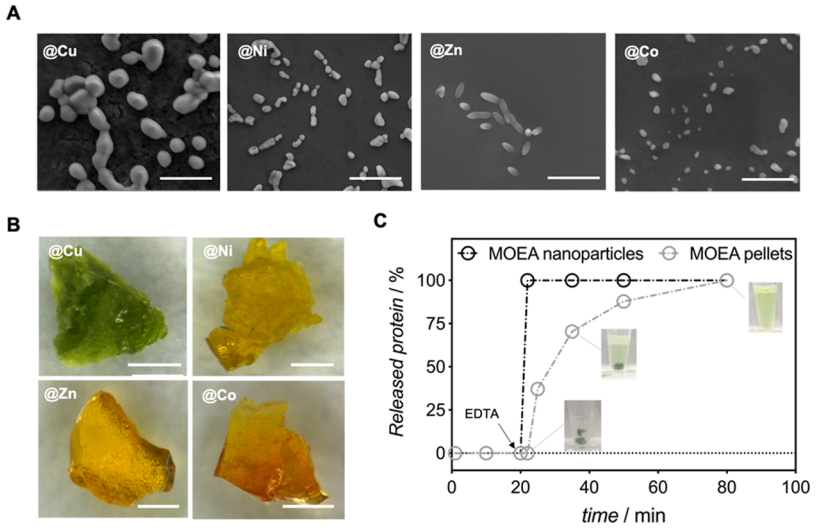

Figure 2. Structural characterization of MOEAs and disassembly in the presence of a complex agent. (A) ESEM pictographs of @Cu, @Ni, @Zn, and @Co MOEA nanoparticles (scale bar: 2 μm). (B) Photographs of @Cu, @Ni, @Zn, and @Cu MOEA pellets (scale bar: 2 mm). (C) Robustness of MOEA nanoparticles and pellets in water and disassembly after addition of 2 mM EDTA (20 min).

within the nanogel is evidenced by the identification of peaks corresponding to the C−H stretching vibrations (3113 cm^{-1}) and the C−N stretching vibrations (1248 cm^{-1}) and the bending (917, 650 cm^{-1}) of the imidazole ring in the GOx@imNG sample.[36] Altogether, we can unequivocally confirm that the GOx enzyme is entrapped in a matrix of poly(AAm-*co*-VIm) hydrogel.

2.2. Synthesis and Characterization of Metal−Organic Enzyme Aggregates. The formation of MOEAs is evidenced by the turbidity of the mixtures after the addition of various metal salts (5 mM) (Scheme 1ii), i.e., $CuSO_4$, $Ni(NO_3)_2$, $Co(NO_3)_2$, or $Zn(NO_3)_2$, to a GOx@imNG solution (0.25 mg mL^{-1}) in Tris buffer (2-amino-2-(hydroxymethyl)propane-1,3-diol, 30 mM, pH 7.0). This demonstrates a fast nanogel bridging provoked by the divalent cations. The suspensions were thoroughly vortexed and stirred for 2 h at room temperature and then the precipitates were washed off with sequential centrifugation/particle suspension steps (see Materials and Methods for details). The presence of respective metal components within the aggregates was confirmed by energy-dispersive X-ray (EDX) spectroscopy (Figure S4). Moreover, this protocol was remarkably efficient in terms of protein immobilization yield (90−97%) (Table S1) and enzyme loadings (30−43%) (Table S2). The aggregates obtained with this protocol are referred to as GOx@Cu, GOx@Ni, GOx@Co, and GOx@Zn MOEAs.

The assessment of metal−imidazole coordination was performed by Raman spectroscopy as reported before (Figure S5).[37] Additionally, herein we demonstrate that ATR-FTIR spectroscopy can be likewise utilized for monitoring such interaction (Figure 1C). By FTIR, the corresponding peaks were found in a cleaner spectral window (915−970 cm^{-1}) in this type of samples. The infrared peak attributed to the torsional bending of the imidazole rings, which in GOx@imNG is settled at 917 cm^{-1}, experiences a shift to higher wavenumbers when the imidazole molecules coordinate to metal cations. This shift relies upon the nature of the metal cation the imidazole is interacting with. Hence, the GOx@Cu sample showed an additional band at 955 cm^{-1}, GOx@Ni at 944 cm^{-1}, GOx@Co at 942 cm^{-1}, and GOx@Zn at 956 cm^{-1}. Moreover, long incubation times (up to 72 h) led to the complete disappearance of the peak at 917 cm^{-1}. Certainly, Zn−imidazole peak detected for GOx@Zn MOEA is in good agreement with that described in the literature for zeolitic imidazolate frameworks, namely, ZIF-8 composites (Figure S6).[38]

The synthesized hybrids rendered nanoparticles of similar size (around 400−900 nm) but diverse morphologies as revealed by environmental scanning electron microscopy (ESEM) and DLS (Figures 2A and S7). Particularly, rounded-ovated (GOx@Cu, GOx@Co), geometrical (GOx@Ni), and petal-shaped (GOx@Zn) structures were observed under ESEM (details in Figure S8). As clearly observed in GOx@Cu particles, but also in GOx@Ni, MOEAs tend to aggregate, making it difficult to identify individual entities. Such a trend for aggregation was pronounced when a higher nanogel concentration of 0.5 mg mL^{-1} was used for the assembly. Larger aggregates, which are homogeneously dispersed in aqueous solution, led to the formation of clusters composed of smaller spherical nanoparticles with sizes of around 150−200 nm according to ESEM (Figure S9). Interestingly, the combination of higher nanogel seeding concentration (2 mg mL^{-1}) with a lower metal cation concentration (0.5 mM) led to rapid aggregation, with the precipitate forming an insoluble and compact pellet that could no longer be dispersed (Figure 2B). All synthesized MOEAs are stable in aqueous solution, yet the cation−imidazole interaction can be disrupted using metal-complexing agents such as ethylenediamidetetraacetic acid (EDTA, Figure 2C). Although MOEA nanoparticles were immediately disassembled in the presence of a 2 mM EDTA solution, the disruption of MOEA pellets was significantly slower (see Material and Methods).

The metal-directed assembly of imidazole nanogels was tested in the presence of different buffer solutions such as water, sodium acetate (30 mM, pH 5.0), and sodium phosphate (30 mM, pH 6.0). According to the FTIR spectra (Figure S10), the assembly in water and acetate buffer rendered MOEAs of similar composition but with lower protein immobilization yields than those fabricated in Tris buffer (<50%, Table S1). Moreover, the dispersion of the assembled particles became difficult. Hence, it seemed that

DOI: 10.1021/acsomega.8b03559
ACS Omega 2019, 4, 5172−5179

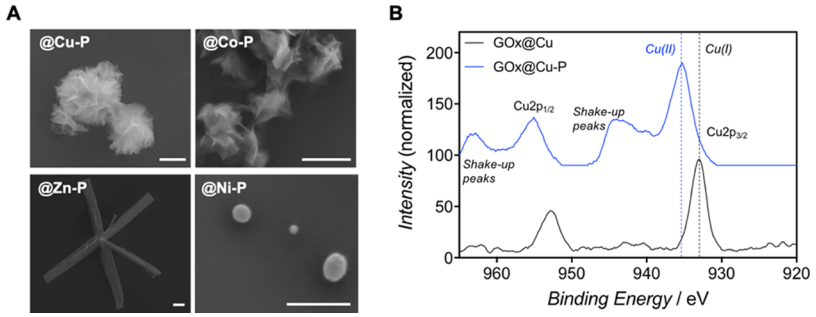

Figure 3. Structural characterization of the hybrids grown in phosphate buffer by ESEM (A) and chemical characterization of Cu component (Cu $2p_{1/2}$ and Cu $2p_{3/2}$) by X-ray photoelectron spectroscopy (XPS) of GOx@Cu-P and GOx@Cu samples (B) (scale bar: 2.5 μm). Dotted lines highlight the position of the maxima of the respective Cu $2p_{3/2}$ peaks.

Table 1. Measured Apparent Catalytic Parameters for GOx MOEAs, @ZIF-8 Composites, and Free GOx

	@Cu	@Co	@Zn	@Ni	@ZIF-8#1	@ZIF-8#2	free
$^{app}K_m$ (mM)[a]	18.8 ± 5.4	15.0 ± 4.1	21.1 ± 6.3	14.9 ± 2.9	30.2 ± 6.7	19.9 ± 2.3	18.0 ± 1.7
$^{app}k_{cat}$ (min^{-1})[a]	22 844 ± 500	10 974 ± 292	9817 ± 114	10 966 ± 189	1193 ± 220	1285 ± 40	30 060 ± 1910
k_{cat}/K_m (mM^{-1} min^{-1})	1218	732	465	735	40	65	1670

[a]Measurements were performed by triplicates at 42 °C using the glucose/HRP/ABTS system described in Materials and Methods section. Glucose and enzyme concentration ranged from 0 to 200 mM and 0 to 9 nM for $^{app}K_m$ and $^{app}k_{cat}$ measurements, respectively.

Tris buffer stabilizes and prompts the formation of MOEAs, as Tris molecules have been reported to coordinate divalent cations.[39,40] Interestingly, the assembly in phosphate buffer led to completely different particles (herein named GOx@Cu-P, GOx@Ni-P, GOx@Co-P, and GOx@Zn-P) from both structural and chemical perspectives (Figures 3A and S11).

A deep spectroscopic characterization of the GOx@Cu and GOx@Cu-P samples was performed using inductively coupled plasma-mass spectrometry (ICP-MS), ATR-FTIR, and X-ray photoelectron spectroscopy (XPS). As collated in Table S2, the ICP-MS measurements showed that the Cu content in GOx@Cu-P was 75 times higher than that in GOx@Cu. Moreover, the detection of the prominent infrared bands corresponding to the asymmetric and symmetric stretching vibrations of PO_4^{3-} (1000−1100 cm^{-1}) by ATR-FTIR (Figure S11), together with the identification of phosphorus as phosphate ion by XPS (Table S3 and Figure S12A), points towards the growth of copper phosphate around the nanogels in the GOx@Cu-P sample. This is consistent with reported organic−inorganic protein hybrids synthesized in phosphate buffered saline (PBS) buffer.[41,42]

A close view to the Cu signal of both GOx@Cu and GOx@Cu-P by XPS (Figure 3B) revealed a clear shift of the Cu $2p_{3/2}$ band from 935.2 to 932.7 eV for the GOx@Cu-P and GOx@Cu samples. Whereas the peak at higher energies corresponds to Cu(II), the lower-energy peak coincides with that typically observed from Cu_3N-based materials.[43] The Cu(I) state within the sample is also noticed by the green appearance of the solid precipitate (Figure S12B).

2.3. Catalytic Performance of MOEAs. Next, the catalytic behavior of MOEAs toward glucose oxidation was tested using glucose/HRP/ABTS detection method (Materials and Methods). GOx-embedded ZIF-8 composites were synthesized and characterized as reference of analogous metal−organic heterogeneous catalysts. As the performance of the ZIF-8−enzyme composites relies on the approach chosen for their synthesis,[20] we selected two methods to encapsulate GOx into zeolitic imidazolate frameworks (Figure S13) and compared them to MOEAs. The first method, used to fabricate GOx@ZIF-8#1 composite, utilizes Brij/cyclohexane/water reverse micelle system for the confinement of the enzyme and reagents in small aqueous volumes.[16] Otherwise, GOx@ZIF-8#2 required the addition of polyvinylpyrrolidone as a capping agent to assist the dispersion and stabilization of protein in methanol.[23] The kinetic characterization of MOEAs and ZIF-8 hybrids showed interesting features, which are listed in Table 1. Overall, all GOx-MOEAs outperformed GOx@ZIF-8s in terms of activity (Figure 4).

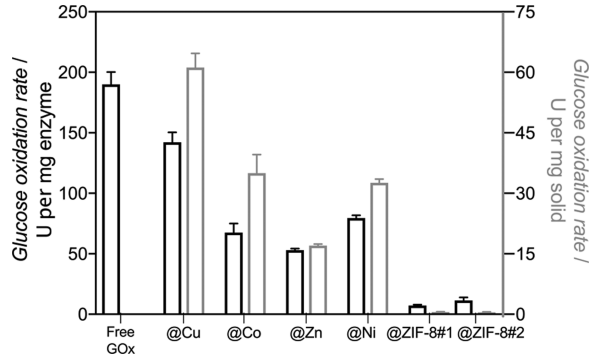

Figure 4. Glucose oxidation activity measurements represented in U (μmol glucose min^{-1}) per mg of enzyme (left axis, in black) and U per mg of solid biocatalyst (right axis, in gray). The activity of free GOx is represented as a reference.

From all measured hybrids, @Cu MOEAs evidenced highest catalytic efficiency, comparable to that showed by free enzyme. This effect might be related to the synergistic effect of GOx and Cu(I) within the hybrid. Indeed, the utilization of Cu(I) derivatives, i.e., Cu_2O, as promising nonenzymatic glucose sensors has been reported.[37] Therefore, in this case, the metal cation works not only as a structural unit but also contributes to the overall catalytic performance of the hybrid.

The analysis of individual kinetics parameters showcased that whereas MOEA and @ZIF-8#2 hybrids had apparent Michaelis constant ($^{app}K_m$) values similar or even lower than

DOI: 10.1021/acsomega.8b03559
ACS Omega 2019, 4, 5172−5179

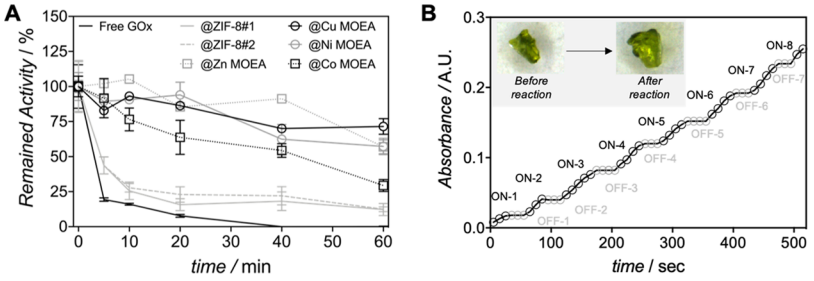

Figure 5. Thermostability and recycling of MOEAs. (A) Glucose oxidation activity monitoring of free GOx enzyme, MOEAs, and @ZIF-8 hybrids at 65 °C and up to 1 h of incubation. For each sample, 100% value was set as their activity at room temperature. (B) On−off switching experiment showing the immersion (ON) and withdrawal (OFF) of GOx@Cu MOEAs into and out of the reaction mixture, respectively. The reaction is monitored by measuring the absorbance at 416 nm. Inset picture shows swollen MOEAs after 10 min of reaction.

those of free GOx, @ZIF-8#1 evidenced a detrimental effect on the affinity toward glucose ($^{app}K_m$ of 30.2 vs 18.0 mM measured for @ZIF-8#1 and free GOx samples, respectively). This effect might be caused by the use of organic solvents, i.e., hexane and detergents, during the synthesis procedure. Moreover, the measurement of apparent turnover numbers ($^{app}k_{cat}$) evidenced more prominent substrate diffusion issues in @ZIF-8-type hybrids with significantly lower turnover values.

The high protein content of GOx-MOEAs, with 30−43% (w/w) of the solid dry weight, contrasts with the highly diluted enzyme within the @ZIF-8 composites (only 8 and 4 wt % of the dry weight measured for @ZIF-8#1 and @ZIF-8#2 samples, respectively) (Table S2). Thus, the presence of huge quantities of inactive material in latter composites leads to a marked dilution of activity per mg of solid catalyst when compared to MOEA hybrids (∼0.5 U per mg of solid catalyst of ZIF-8 hybrids vs 17−60 U per mg of catalyst measured for MOEAs) (Figure 4). Same detrimental effect was found with @Zn-P, @Cu-P, @Ni-P, and @Co-P samples, which showed a loss of 48, 80, 70, and 80%, respectively, of the activity measured for their respective MOEA ion counterparts (Figure S14).

2.4. Thermostability and Reusability of MOEAs. The success of MOEAs as heterogeneous catalysts is dependent on the possibility to be used under harsh operational conditions and in cyclic reactions with minimal activity loss. We hypothesized that the embedment of GOx into a polymeric network and ulterior assembly into a supramolecular structure might protect the enzyme from denaturation at high temperatures. Therefore, we checked the thermostability of MOEAs by monitoring the biocatalytic activity after being heated at 65 °C for 1 h. This temperature was selected because we expected that the protein confinement into polymer nanogels would hamper the loss of the tertiary structure, which takes place at >50 °C (T_m of 60 °C) (Figure S15).

As depicted in Figure 5A, only GOx hybrids showed activity after 1 h at 65 °C. However, the stability profile was completely different for both types materials. This disparity in thermostability was remarkable when hybrids built through Zn(II)−imidazole coordination, i.e., GOx@Zn and GOx@ZIF-8, were compared. GOx@ZIF-8 lost ∼75% of the activity after 10 min at 65 °C and then the catalytic rate was kept almost constant for 50 min. Otherwise, @Zn MOEAs conserved nearly intact (∼100 to 80%) their ability to oxidize glucose for 40 min, and we observe a loss of 40% of the activity only in the final stage of incubation. These results demonstrate that the metal−organic component in MOEAs, i.e., the polymer coating, provides significant protection to enzyme against protein denaturation at high temperatures.

The use of MOEAs in cyclic reactions was studied with the ON−OFF switching activity assay using large-pellet MOEAs, since pellets can be easily taken out from the reaction solution (Figure 5B). We started the reaction by the immersion (ON phase) of pellets into the reaction solution and stopped the reaction by the removal of those (OFF phase) to test the performance of MOEAs in sequential cyclic reactions. This process was repeated 8 times to have 8 reaction cycles. We observed that the reaction stopped completely upon the withdrawal of MOEAs and the integrity and associated activity of the MOEAs is retained throughout the switching sequence. Moreover, we observed a steady catalytic rate all along the experiment. Thus, we demonstrated that even though the pellets were clearly swollen, there was no protein leakage neither enzyme inactivation along the 8 sequential cycles.

3. CONCLUSIONS

In summary, a clear benefit is given by the utility of metal−imidazole coordination for the confinement of proteins and the eventual formation of a new sort of metal−organic enzyme hybrids. The presented methodology shows the first reported example of the addition of imidazole co-monomers in a copolymer−enzyme mixture for the one-pot synthesis of imidazole-decorated enzyme−polymer nanoconjugates. The metal-directed assembly of such conjugates derived into catalytically highly active and excellently tunable metal−organic enzyme hybrids, meaning that MOEAs can be tailored (in terms of morphology and/or composition) a priori in accordance with specific applications. A comparison with other reported metal−organic enzyme hybrids, i.e., enzyme−ZIF-8 composites, revealed MOEAs as heterogeneous catalysts with low diffusional issues and high protein loads. The synergistic effect of Cu(I) and GOx on glucose oxidation prompted GOx@Cu as the most active hybrids assayed in this work. Indeed, we measured up to a 122-fold enhancement of the glucose oxidation rate per mg of catalyst. Moreover, we observed a marked thermostability of @Zn MOEA hybrids, presumably due to the joint protection provided by the polymeric network and the metal-driven supramolecular assembly. Altogether, high activity and protein loads, great thermostability, and reusability make MOEAs an excellent alternative as carrierless immobilization system.

4. MATERIALS AND METHODS

4.1. Materials. Acrylamide (AAm; 99.9%, Sigma), *N*,*N*′-methylenebisacrylamide (MBAAm; >99%, Sigma), vinyl

DOI: 10.1021/acsomega.8b03559
ACS Omega 2019, 4, 5172−5179

imidazole (VIm, >99%, Sigma), ammonium persulfate (APS; 98%, Sigma), tetramethylethylenediamine (TEMED; 99%, Sigma), 2,2′-azino-bis(3-ethylbenzothiazoline-6-sulphonic acid) (ABTS; Panreac AppliChem), hydrogen peroxide (35% v/v in water, Carl Roth), D-glucose (≥95%, Carl Roth), and glucose oxidase from *Aspergillus niger* (GOx; E.C. 1.1.3.4, 108 U per mg, Amresco) were used. Unless specified otherwise, solvents were of analytical grade and purchased from VWR or Fisher Scientific. All buffers were freshly prepared and filtered through 0.22 μm filters prior to use. Filter membranes (30 and 10 KDa MWCO, Vivaspin 6, Sartorius), dialysis membranes (10 KDa MWCO, Spectra/Por 6, SpectrumLabs), and HisPur NTA−Ni resin (Thermofisher) were used for the concentration and purification of enzymes and nanogels.

4.2. Methods. The topography of the nanogels was characterized with an AFM 5500, Agilent Technologies/Keysight Technologies in AC mode using a silicon tip with a force constant of 40 N m^{-1} and a resonant frequency of approximately 300 kHz. Height, phase, and amplitude images were recorded simultaneously. AFM images were taken at several positions to be sure that they were representative for the sample surface. All data were processed with Gwyddion 2.31 program. DLS measurements were performed on a Malvern Zetasizer Nano ZS. Experiments were performed at 22 °C and 13 readouts were taken in three independent measurements for each sample. Morphological characterization and EDX analysis were done with an environmental scanning electron microscope (FEI, Quanta 250 FEG) and an Octane Elect EDS (AMETEK) detector at 5.0 kV and 4.5 spot size. The secondary structure of the samples was measured by circular dichroism, using a Jasco J-815 spectropolarimeter at 0.1 nm increments, 10 nm min^{-1} of speed, and 32 s of integration time over a wavelength range of 190−260 nm. Each spectrum represented an accumulation of 5 scans. The FTIR spectra were measured with a PerkinElmer Frontier spectrometer equipped with an ATR sampling stage. All spectra were measured with 20 scans from 600 to 4000 cm^{-1} at 4 cm^{-1} resolution. Each sample was measured 3 times, and the results were averaged. The Cu composition in the nanohybrids was measured with an inductively coupled plasma-mass spectrometer (ICP-MS, NexION 300, Perkin Elmer Inc.) and the data were acquired using the NeoxION software. KED mode was used to avoid signal interferences. XPS experiments were performed in a SPECS Sage HR 100 spectrometer with a non-monochromatic aluminum X-ray source (Kα 1486.6 eV). The selected resolution for the high-resolution spectra was 1.1 eV, measured on a clean silver surface and defined as the full width at half-maximum of the Ag $3d_{5/2}$ peak, with 15 eV of pass energy and 0.15 eV/step and source power of 300 W. Measurements were made in an ultrahigh-vacuum chamber at a pressure around 5×10^{-6} Pa. An electron flood gun was used to neutralize charging.

4.3. Synthesis of GOx@imNG. Imidazole-modified single-enzyme nanogels were synthesized in a single step. Encapsulation of GOx was performed following a protocol based on the conditions described earlier.[44] GOx enzyme (3.6 mg mL^{-1}, 22.5 μM, in sodium phosphate 30 mM buffer, pH 6.1) was mixed with acrylamide (AAm, AAm/GOx 6000:1, n/n), *N*,*N*′-methylenebisacrylamide (MBAAm, MBAAm/GOx 1000:1, n/n), vinyl imidazole (VIm, VIm/GOx 1000:1, n/n), and ammonium persulfate (APS/protein 500:1, n/n). Sucrose (5%, w/v) and dimethyl sulfoxide (10% v/v, 33 mM) were added. This mixture was deoxygenated by bubbling N_2 through the solutions for 45 min. Polymerization reaction started upon addition of N,N,N′,N′-tetramethylenediamine (TEMED, TEMED/APS 2:1, w/w). The reaction was kept under N_2 and shaken at room temperature for 2 h. GOx nanogels were dialyzed against PBS buffer to remove low-molar-mass reagents and passed through a Sephadex G-75 column to remove nonencapsulated enzymes and protein-free polymer hydrogels. Imidazole nanogels were further purified through Ni−NTA agarose affinity columns.

4.4. Calculation of Protein Immobilization Yield and Weight Content. The amount of protein that is incorporated into the nanohybrid-immobilized protein is calculated by measuring the GOx concentration in the solution before and after the assembly. Native protein concentrations were determined with a NanoDropTM spectrophotometer by measuring the absorbance at 450 nm using UV-transparent quartz cuvettes with a 1 cm path length (ε = 28 200 M^{-1} cm^{-1}). The protein weight content (%, w/w, in dried solid) was calculated by gravimetry using dry MOEA solutions of known GOx concentration (40 μL, ∼3.0 mg mL^{-1}).

4.5. Activity Measurements. Standard activity assays were performed at 37 °C in 96-well plates, with 200 μL as the final volume per well unless otherwise mentioned in the text. Unless otherwise mentioned in the text, GOx activity measurement was performed using 6 ng of GOx, 1.0 mM glucose in 30 mM sodium phosphate pH 6.0 with 2,2′-azino-bis(3-ethylbenzothiazoline-6-sulphonic acid) (ABTS) 1 mM and 0.1 ng mL^{-1} of HRP. Color development from oxidized ABTS was monitored in the spectrophotometer at 416 nm. A molar attenuation coefficient of 36 000 M^{-1} cm^{-1} was used for the calculations.

4.6. Kinetic Characterization. Catalytic parameters, $^{app}K_m$ and $^{app}k_{cat}$, were measured by triplicate at 42 °C using the aforementioned glucose/HRP/ABTS system. Measurements were carried out in time course mode by monitoring the absorbance change of oxidized ABTS at 416 nm in the presence of GOx. For that, a UV−vis spectrophotometer (Epoch2, Biotech) was used. The apparent Michaelis−Menten constant ($^{app}K_m$) was calculated by changing the glucose concentration in each well from 0 to 200 mM. The apparent turnover number ($^{app}k_{cat}$) was determined by varying the enzyme concentration in each well from 0 to 9 nM, setting the substrate (glucose) concentration to 100 mM. For the calculations, a molar extinction coefficient for oxidized ABTS of 36 000 M^{-1} cm^{-1} at 416 nm was used in every case.

4.7. Disassembly of MOEAs with EDTA. MOEA nanoparticles and pellets (∼2 to 5 mg) were incubated in water for 20 min. Every 5 min, the samples were centrifuged (8000 rpm, 5 min) and the protein content in the supernatant measured at 450 nm. Thereafter, EDTA (2 mM, final concentration) was added to both solutions, which were centrifuged 2, 5, 10, 30, and 40 min after the addition of the complexing agent. The protein content of the supernatants after centrifugation was measured for each timepoint.

4.8. Thermostability Measurements. The thermostability of nonmodified GOx and biohybrids was checked by incubating the samples (100 μL, 2 μg mL^{-1}) at 65 °C in deionized water. At different time intervals (0, 5, 10, 20, 40, and 60 min), sample aliquots were taken, cooled down, and the activity tested. The residual activity was measured as described above.

DOI: 10.1021/acsomega.8b03559
ACS Omega 2019, 4, 5172−5179

■ ASSOCIATED CONTENT

Supporting Information

The Supporting Information is available free of charge on the ACS Publications website at DOI: 10.1021/acsomega.8b03559.

Structural and functional characterization of protein−polymer conjugates, MOEAs, and ZIF-8 enzyme composites (PDF)

■ AUTHOR INFORMATION

Corresponding Author

*E-mail: a.beloqui@nanogune.eu.

ORCID

Mato Knez: 0000-0002-9850-1035

Ana Beloqui: 0000-0002-7693-4163

Present Address

§CICenergiGUNE, Parque Tecnológico de Álava; Albert Einstein 48, 01510 Miñano, Spain (M.C.M.-M.).

Author Contributions

The manuscript was written through contributions of all authors. All authors have given approval to the final version of the manuscript.

Funding

This project has received funding from the Spanish Ministry of Economy and Competitiveness (MINECO) and FEDER funds in the frame of "Plan Nacional—Retos para la Sociedad" call with the grant reference MAT2017-88808-R. This work was performed under the Maria de Maeztu Units of Excellence Programme—MDM-2016-0618. A.B. thanks Diputación de Guipúzcoa for current funding in the frame of Gipuzkoa Fellows program. M.K. acknowledges the financial support by the Spanish Ministry of Economy and Competitiveness (MINECO) within the grant agreement MAT2016-77393-R, including FEDER funds.

Notes

The authors declare no competing financial interest.

■ ACKNOWLEDGMENTS

We thank Dr Luis Yate for XPS measurements.

■ REFERENCES

(1) Saboe, P. O.; Conte, E.; Farell, M.; Bazan, G. C.; Kumar, M. Biomimetic and Bioinspired Approaches for Wiring Enzymes to Electrode Interfaces. *Energy Environ. Sci.* **2017**, *10*, 14−42.

(2) Aumiller, W. M.; Uchida, M.; Douglas, T. Protein Cage Assembly across Multiple Length Scales. *Chem. Soc. Rev.* **2018**, *47*, 3433−3469.

(3) Yang, X.-Y.; Chen, L.-H.; Li, Y.; Rooke, J. C.; Sanchez, C.; Su, B.-L. Hierarchically Porous Materials: Synthesis Strategies and Structure Design. *Chem. Soc. Rev.* **2017**, *46*, 481−558.

(4) Zdarta, J.; Meyer, A.; Jesionowski, T.; Pinelo, M. A General Overview of Support Materials for Enzyme Immobilization: Characteristics, Properties, Practical Utility. *Catalysts* **2018**, *8*, 92.

(5) Beloqui, A.; Baur, S.; Trouillet, V.; Welle, A.; Madsen, J.; Bastmeyer, M.; Delaittre, G. Single-Molecule Encapsulation: A Straightforward Route to Highly Stable and Printable Enzymes. *Small* **2016**, *12*, 1716−1722.

(6) Wang, Y.; Hou, C.; Zhang, Y.; He, F.; Liu, M.; Li, X. Preparation of Graphene Nano-Sheet Bonded PDA/MOF Microcapsules with Immobilized Glucose Oxidase as a Mimetic Multi-Enzyme System for Electrochemical Sensing of Glucose. *J. Mater. Chem. B* **2016**, *4*, 3695−3702.

(7) Cipolatti, E. P.; Valério, A.; Henriques, R. O.; Moritz, D. E.; Ninow, J. L.; Freire, D. M. G.; Manoel, E. A.; Fernandez-Lafuente, R.; De Oliveira, D. Nanomaterials for Biocatalyst Immobilization-State of the Art and Future Trends. *RSC Adv.* **2016**, *6*, 104675−104692.

(8) Coscolín, C.; Beloqui, A.; Martínez-Martínez, M.; Bargiela, R.; Santiago, G.; Blanco, R. M.; Delaittre, G.; Márquez-Álvarez, C.; Ferrer, M. Controlled Manipulation of Enzyme Specificity through Immobilization-Induced Flexibility Constraints. *Appl. Catal., A* **2018**, *565*, 59−67.

(9) Zhou, Z.; Hartmann, M. Progress in Enzyme Immobilization in Ordered Mesoporous Materials and Related Applications. *Chem. Soc. Rev.* **2013**, *42*, 3894.

(10) Jehle, F.; Fratzl, P.; Harrington, M. J. Metal-Tunable Self-Assembly of Hierarchical Structure in Mussel-Inspired Peptide Films. *ACS Nano* **2018**, *12*, 2160−2168.

(11) Sanghamitra, N. J. M.; Ueno, T. Expanding Coordination Chemistry from Protein to Protein Assembly. *Chem. Commun.* **2013**, *49*, 4114−4126.

(12) Wiester, M. J.; Ulmann, P. A.; Mirkin, C. A. Enzyme Mimics Based upon Supramolecular Coordination Chemistry. *Angew. Chem., Int. Ed.* **2011**, *50*, 114−137.

(13) Salgado, E. N.; Radford, R. J.; Tezcan, F. A. Metal-Directed Protein Self-Assembly. *Acc. Chem. Res.* **2010**, *43*, 661−672.

(14) Keller, D.; Beloqui, A.; Martínez-Martínez, M.; Ferrer, M.; Delaittre, G. Nitrilotriacetic Amine-Functionalized Polymeric Core-Shell Nanoparticles as Enzyme Immobilization Supports. *Biomacromolecules* **2017**, *18*, 2777−2788.

(15) Cassimjee, K. E.; Hendil-Forssell, P.; Volkov, A.; Krog, A.; Malmo, J.; Aune, T. E. V.; Knecht, W.; Miskelly, I. R.; Moody, T. S.; Svedendahl Humble, M. Streamlined Preparation of Immobilized Candida Antarctica Lipase B. *ACS Omega* **2017**, *2*, 8674−8677.

(16) Lyu, F.; Zhang, Y.; Zare, R. N.; Ge, J.; Liu, Z. One-Pot Synthesis of Protein-Embedded Metal-Organic Frameworks with Enhanced Biological Activities. *Nano Lett.* **2014**, *14*, 5761−5765.

(17) Wu, X.; Ge, J.; Yang, C.; Hou, M.; Liu, Z. Facile Synthesis of Multiple Enzyme-Containing Metal−Organic Frameworks in a Biomolecule- Friendly Environment. *Chem. Commun.* **2015**, *51*, 13408−13411.

(18) Cui, J.; Ren, S.; Sun, B.; Jia, S. Optimization Protocols and Improved Strategies for Metal-Organic Frameworks for Immobilizing Enzymes: Current Development and Future Challenges. *Coord. Chem. Rev.* **2018**, *370*, 22−41.

(19) Lian, X.; Fang, Y.; Joseph, E.; Wang, Q.; Li, J.; Banerjee, S.; Lollar, C.; Wang, X.; Zhou, H.-C. Enzyme−MOF (Metal−Organic Framework) Composites. *Chem. Soc. Rev.* **2017**, *46*, 3386−3401.

(20) Liang, W.; Ricco, R.; Maddigan, N. K.; Dickinson, R. P.; Xu, H.; Li, Q.; Sumby, C. J.; Bell, S. G.; Falcaro, P.; Doonan, C. J. Control of Structure Topology and Spatial Distribution of Biomacromolecules in Protein@ZIF-8 Biocomposites. *Chem. Mater.* **2018**, *30*, 1069−1077.

(21) Zhu, Q.; Zhuang, W.; Chen, Y.; Wang, Z.; Villacorta Hernandez, B.; Wu, J.; Yang, P.; Liu, D.; Zhu, C.; Ying, H.; et al. Nano-Biocatalysts of Cyt C@ZIF-8/GO Composites with High Recyclability via a de Novo Approach. *ACS Appl. Mater. Interfaces* **2018**, *10*, 16066−16076.

(22) Doonan, C.; Riccò, R.; Liang, K.; Bradshaw, D.; Falcaro, P. Metal-Organic Frameworks at the Biointerface: Synthetic Strategies and Applications. *Acc. Chem. Res.* **2017**, *50*, 1423−1432.

(23) Chulkaivalsucharit, P.; Wu, X.; Ge, J. Synthesis of Enzyme-Embedded Metal-Organic Framework Nanocrystals in Reverse Micelles. *RSC Adv.* **2015**, *5*, 101293−101296.

(24) Ouyang, G.; Chen, G.; Huang, S.; Kou, X.; Wei, S.; Huang, S.; Jiang, S.; Shen, J.; Zhu, F. A Convenient and Versatile Amino Acid-Boosted Biomimetic Strategy for Nondestructive Encapsulation of Biomacromolecules within Metal−Organic Framework. *Angew. Chem., Int. Ed.* **2019**, *58*, 1463−1467.

(25) Naseri, M.; Pitzalis, F.; Carucci, C.; Medda, L.; Fotouhi, L.; Magner, E.; Salis, A. Lipase and Laccase Encapsulated on Zeolite Imidazolate Framework: Enzyme Activity and Stability from Voltammetric Measurements. *ChemCatChem* **2018**, *10*, 5425−5433.

DOI: 10.1021/acsomega.8b03559
ACS Omega 2019, 4, 5172−5179

(26) Chen, W. H.; Vázquez-González, M.; Zoabi, A.; Abu-Reziq, R.; Willner, I. Biocatalytic Cascades Driven by Enzymes Encapsulated in Metal−Organic Framework Nanoparticles. *Nat. Catal.* **2018**, *1*, 689−695.
(27) Murata, H.; Carmali, S.; Baker, S. L.; Matyjaszewski, K.; Russell, A. J. Solid-Phase Synthesis of Protein-Polymers on Reversible Immobilization Supports. *Nat. Commun.* **2018**, *9*, No. 845.
(28) Cummings, C.; Murata, H.; Koepsel, R.; Russell, A. J. Tailoring Enzyme Activity and Stability Using Polymer-Based Protein Engineering. *Biomaterials* **2013**, *34*, 7437−7443.
(29) Beloqui, A.; Kobitski, A. Y.; Nienhaus, G. U.; Delaittre, G. A Simple Route to Highly Active Single-Enzyme Nanogels. *Chem. Sci.* **2018**, *9*, 1006−1013.
(30) Stepankova, V.; Bidmanova, S.; Koudelakova, T.; Prokop, Z.; Chaloupkova, R.; Damborsky, J. Strategies for Stabilization of Enzymes in Organic Solvents. *ACS Catal.* **2013**, *3*, 2823−2836.
(31) Velonia, K. Protein-Polymer Amphiphilic Chimeras: Recent Advances and Future Challenges. *Polym. Chem.* **2010**, *1*, 944−952.
(32) Sheldon, R. A.; van Pelt, S. Enzyme Immobilisation in Biocatalysis: Why, What and How. *Chem. Soc. Rev.* **2013**, *42*, 6223−6235.
(33) Jang, J.; Park, H. Formation and Structure of Polyacrylamide-Silica Nanocomposites by Sol-Gel Process. *J. Appl. Polym. Sci.* **2002**, *83*, 1817−1823.
(34) Zhang, F.; Wang, M.; Liang, C.; Jiang, H.; Shen, J.; Li, H. Thin-Layer Polymer Wrapped Enzymes Encapsulated in Hierarchically Mesoporous Silica with High Activity and Enhanced Stability. *Sci. Rep.* **2014**, *4*, No. 4421.
(35) Murugan, R.; Mohan, S.; Bigotto, A. FTIR and Polarized Raman Spectra of Acrylamide and Polyacrylamide. *J. Korean Phys. Soc.* **1998**, *32*, 505−512.
(36) Ramasamy, R. Vibrational Spectroscopic Studies of Imidazole. *Arm. J. Phys.* **2015**, *8*, 51−55.
(37) Takeuchi, H. Raman Structural Markers of Tryptophan and Histidine Side Chains in Proteins. *Biopolymers* **2003**, *72*, 305−317.
(38) Yin, Y.; Xiao, Y.; Lin, G.; Xiao, Q.; Lin, Z.; Cai, Z. An Enzyme−Inorganic Hybrid Nanoflower Based Immobilized Enzyme Reactor with Enhanced Enzymatic Activity. *J. Mater. Chem. B* **2015**, *3*, 2295−2300.
(39) Colombo, M. F.; Austrilino, L.; Nascimento, O. R.; Castellano, E. E.; Tabak, M. On the Interaction of Copper with Tris-(Hydroxymethyl)Aminomethane. *Can. J. Chem.* **1987**, *65*, 821−826.
(40) Fischer, B. E.; Haring, U. K.; Tribolet, R.; Sigel, H. Metal Ion/Buffer Interactions. *Eur. J. Biochem.* **1979**, *94*, 523−530.
(41) Rodriguez-Abetxuko, A.; Morant-Miñana, M. C.; López-Gallego, F.; Yate, L.; Seifert, A.; Knez, M.; Beloqui, A. Imidazole-Grafted Nanogels for the Fabrication of Organic−Inorganic Protein Hybrids. *Adv. Funct. Mater.* **2018**, *28*, No. 1803115.
(42) Ge, J.; Lei, J.; Zare, R. N. Protein−Inorganic Hybrid Nanoflowers. *Nat. Nanotechnol.* **2012**, *7*, 428−432.
(43) Meng, F. L.; Zhong, H. X.; Zhang, Q.; Liu, K. H.; Yan, J. M.; Jiang, Q. Integrated Cu3N Porous Nanowire Array Electrode for High-Performance Supercapacitors. *J. Mater. Chem. A* **2017**, *5*, 18972−18976.
(44) Beloqui, A.; Baur, S.; Trouillet, V.; Welle, A.; Madsen, J.; Bastmeyer, M.; Delaittre, G. Single-Molecule Encapsulation: A Straightforward Route to Highly Stable and Printable Enzymes. *Small* **2016**, *12*, 1716−1722.

DOI: 10.1021/acsomega.8b03559
ACS Omega 2019, 4, 5172−5179